

NEUTRON-STAR RADIUS CONSTRAINTS FROM GW170817 AND FUTURE DETECTIONS

ANDREAS BAUSWEIN,¹ OLIVER JUST,² HANS-THOMAS JANKA,³ AND NIKOLAOS STERGIIOULAS⁴

¹*Heidelberger Institut für Theoretische Studien, Schloss-Wolfsbrunnengasse 35, D-69118 Heidelberg, Germany*

²*Astrophysical Big Bang Laboratory, RIKEN, Saitama 351-0198, Japan*

³*Max-Planck-Institut für Astrophysik, Karl-Schwarzschild-Str. 1, D-85748 Garching, Germany*

⁴*Department of Physics, Aristotle University of Thessaloniki, GR-54124 Thessaloniki, Greece*

(Received July 1, 2016; Revised September 27, 2016; Accepted May 22, 2022)

Submitted to ApJL

ABSTRACT

We introduce a new, powerful method to constrain properties of neutron stars (NSs). We show that the total mass of GW170817 provides a reliable constraint on the stellar radius if the merger did not result in a prompt collapse as suggested by the interpretation of associated electromagnetic emission. The radius $R_{1.6}$ of nonrotating NSs with a mass of $1.6 M_{\odot}$ can be constrained to be larger than $10.68^{+0.15}_{-0.04}$ km, and the radius R_{\max} of the nonrotating maximum mass configuration must be larger than $9.60^{+0.14}_{-0.03}$ km. We point out that detections of future events will further improve these constraints. Moreover, we show that a future event with a signature of a prompt collapse of the merger remnant will establish even stronger constraints on the NS radius from above and the maximum mass M_{\max} of NSs from above. These constraints are particularly robust because they only require a measurement of the chirp mass and a distinction between prompt and delayed collapse of the merger remnant, which may be inferred from the electromagnetic signal or even from the presence/absence of a ringdown gravitational-wave (GW) signal. This prospect strengthens the case of our novel method of constraining NS properties, which is directly applicable to future GW events with accompanying electromagnetic counterpart observations. We emphasize that this procedure is a new way of constraining NS radii from GW detections independent of existing efforts to infer radius information from the late inspiral phase or postmerger oscillations, and it does not require particularly loud GW events.

Keywords: gravitational waves — stars: neutron — equation of state

1. INTRODUCTION

The recently detected GW170817 is the first observed gravitational-wave (GW) source involving matter and the first with strong evidence for accompanying electromagnetic emission [Abbott et al. \(2017\)](#); [LIGO Scientific Collaboration et al. \(2017\)](#). The measured binary masses are only compatible with a neutron-star (NS) merger. Apart from the importance of this detection for stellar astrophysics and nucleosynthesis, such events are highly interesting because they bear the potential to infer weakly-constrained properties of NSs ([Lattimer & Prakash 2016](#); [Özel & Freire 2016](#); [Oertel et al. 2017](#)). Such information can be obtained from the GW signal either from finite-size effects during the late inspiral phase prior to merging (e.g. [Faber et al. 2002](#); [Flanagan & Hinderer 2008](#); [Read et al. 2013](#); [Del Pozzo et al. 2013](#); [Abbott et al. 2017](#)) or through the characteristic oscillations of the postmerger remnant (e.g. [Bauswein & Janka 2012](#); [Bauswein et al. 2012, 2014](#); [Takami et al. 2014](#); [Clark et al. 2014](#); [Chatziioannou et al. 2017](#)). Both approaches require high signal-to-noise ratios (SNRs). The relative proximity of GW170817 and the therefore presumably high NS merger rate suggest that such measurements might be possible already in the era of the current GW detectors.

The merging of two NSs can result either in the direct formation of a black hole (BH) (prompt collapse) or the formation of an at least transiently stable NS merger remnant (delayed/no collapse). The former case occurs for mergers with binary masses M_{tot} above a threshold binary mass M_{thres} , a delayed or no collapse results for binaries with $M_{\text{tot}} < M_{\text{thres}}$. The two different collapse scenarios are also expected to lead to different electromagnetic emission. On the one hand, the amount of dynamical ejecta is strongly reduced in the case of prompt BH formation ([Bauswein et al. 2013b](#); [Hotokezaka et al. 2013](#)). Moreover, the different nature of the merger remnant yields different amounts of secular ejecta ([Fernández & Metzger 2013](#); [Metzger & Fernández 2014](#); [Perego et al. 2014](#); [Siegel et al. 2014](#); [Just et al. 2015](#)).

In this letter we present a new method to infer information on the NS equation of state (EoS) from NS mergers that does not require a high SNR of the GW measurement. Our constraint only relies on the measured binary mass of GW170817 and the evidence for a delayed/no collapse in this event as suggested by its electromagnetic emission (e.g. [Kasen et al. 2017](#); [Metzger 2017](#)). In the case of a delayed/no collapse the measured total binary mass of GW170817 provides a lower

bound on the threshold mass for direct BH formation,

$$M_{\text{thres}} > M_{\text{tot}}^{\text{GW170817}} = 2.74_{-0.01}^{+0.04} M_{\odot}, \quad (1)$$

and we conclude that the radius $R_{1.6}$ of a NS with $1.6 M_{\odot}$ must be larger than $10.68_{-0.04}^{+0.15}$ km. We demonstrate that our new method promises very strong constraints on NS radii and the maximum mass M_{max} of nonrotating NSs if more NS mergers will be observed and in particular if an event with a prompt collapse of the merger remnant is identified.

2. OBSERVATIONS

Several telescopes observed emission in the X-ray, optical and infrared from the GW source with spatial and temporal coincidence ([LIGO Scientific Collaboration et al. 2017](#)). The observations are compatible with NS merger ejecta that are heated by the nuclear decays of products of the rapid neutron-capture process ([Metzger et al. 2010](#)). The light-curve properties were interpreted as being produced by dynamical ejecta from the merger and secular ejecta from the merger remnant. The estimated ejecta mass is in the range 0.03 to $0.05 M_{\odot}$ ([Cowperthwaite et al. 2017](#); [Kasen et al. 2017](#); [Nicholl et al. 2017](#); [Chornock et al. 2017](#); [Drout et al. 2017](#); [Smartt et al. 2017](#); [Kasliwal et al. 2017](#); [Kilpatrick et al. 2017](#); [Tanvir et al. 2017](#); [Tanaka et al. 2017](#)), which even for asymmetric binaries lies near the high end of the theoretical range expected from simulations. This can be interpreted as tentative evidence for a delayed/no collapse in GW170817 because this merger outcome tends to produce larger ejecta masses as compared to a direct collapse, and neutrino irradiation by the merger remnant increases the electron fraction yielding a blue component ([Bauswein et al. 2013b](#); [Hotokezaka et al. 2013](#); [Fernández & Metzger 2013](#); [Metzger & Fernández 2014](#); [Perego et al. 2014](#); [Siegel et al. 2014](#); [Wanajo et al. 2014](#); [Just et al. 2015](#); [Sekiguchi et al. 2016](#)). We thus use below the assumption of no prompt collapse in GW170817 and leave the detailed interpretation of the electromagnetic emission to future work. Our assumption can be corroborated by refined models and future observations.

3. NEUTRON-STAR RADIUS CONSTRAINTS

3.1. Threshold binary mass

If GW170817 resulted in a delayed collapse or no collapse, its total mass provides a lower limit on the threshold binary mass for prompt collapse as given by Eq. (1).

The threshold binary mass M_{thres} depends sensitively on the EoS ([Shibata 2005](#); [Baiotti et al. 2008](#); [Hotokezaka et al. 2011](#); [Bauswein et al. 2013a](#)). Considering different EoSs, in [Bauswein et al. \(2013a\)](#) we found

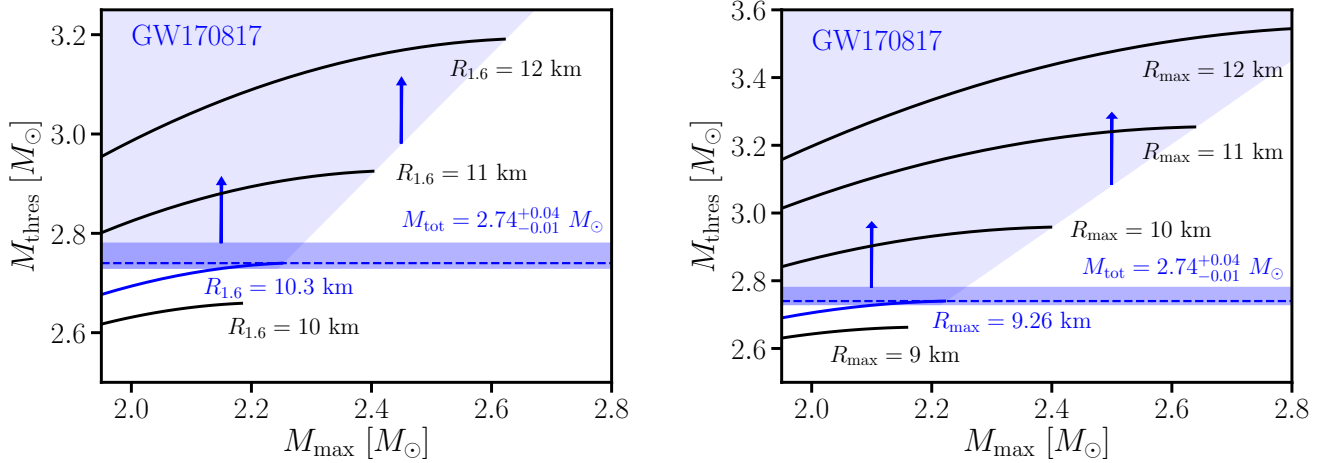


Figure 1. Threshold binary mass M_{thres} for prompt collapse as function of M_{max} for different $R_{1.6}$ (left panel, Eq. 2) and R_{max} (right panel, Eq. 3) (solid lines). The dark blue band shows the total binary mass of GW170817. This provides a lower limit on M_{thres} . The true threshold binary mass must lie within the light blue areas if GW170817 resulted in a delayed/no collapse. This rules out NSs with $R_{1.6} \leq 10.30^{+0.18}_{-0.03}$ km and $R_{\text{max}} \leq 9.26^{+0.17}_{-0.03}$ km. Causality requires $M_{\text{thres}} \geq 1.22M_{\text{max}}$ (left panel) and $M_{\text{thres}} \geq 1.23M_{\text{max}}$ (right panel)

by hydrodynamical simulations that the threshold binary mass to good accuracy follows

$$M_{\text{thres}} = \left(-3.606 \frac{GM_{\text{max}}}{c^2 R_{1.6}} + 2.38 \right) \cdot M_{\text{max}} \quad (2)$$

with $R_{1.6}$ being the radius of a nonrotating NS with a mass of $1.6 M_{\odot}$ and M_{max} being the maximum mass of nonrotating NSs. The relation was derived from simulations of symmetric binary mergers but also holds for moderately asymmetric systems (Bauswein et al. 2013a; Bauswein & Stergioulas 2017). We verify by additional simulations that strongly asymmetric mergers with mass ratio $q = 0.6$ have a threshold binary mass which is systematically lower by 0.1 to 0.3 M_{\odot} than M_{thres} of equal-mass binaries. This reduction of M_{thres} for asymmetric binaries is understandable. The heavier binary component forming the core of the merger remnant moves more slowly on its orbit and thus the specific angular momentum in the core is relatively low, which results in less stabilization. If GW170817 was very asymmetric, one has $M_{\text{thres}}^{\text{asym}} \geq M_{\text{tot}}$, which implies that Eq. (1) is conservative because $M_{\text{thres}} > M_{\text{thres}}^{\text{asym}}$ for a given $R_{1.6}$. Avoiding a prompt collapse in the asymmetric case would require an even larger value of $R_{1.6}$ than for symmetric mergers.

A similarly accurate description of M_{thres} is given by the fit

$$M_{\text{thres}} = \left(-3.38 \frac{GM_{\text{max}}}{c^2 R_{\text{max}}} + 2.43 \right) \cdot M_{\text{max}} \quad (3)$$

with the radius R_{max} of the maximum-mass configuration. Eq. (2) is accurate to better than 0.1 M_{\odot} (see Bauswein et al. (2013a, 2016) for details). The existence

of these relations has been solidified by semi-analytic calculations of equilibrium models (Bauswein & Stergioulas 2017).

3.2. Radius constraints

Equations (2) and (3) imply constraints on NS radii $R_{1.6}$ and R_{max} since the total binary mass of GW170817 represents a lower bound on M_{thres} (Eq. (1)). Figure 1 (left panel) shows $M_{\text{thres}}(M_{\text{max}}; R_{1.6})$ (Eq. (2)) for different chosen values of $R_{1.6}$ (solid lines). Every sequence terminates at

$$M_{\text{max}} = \frac{1}{3.10} c^2 R_{1.6} / G, \quad (4)$$

which is a safe upper limit on M_{max} for the given $R_{1.6}$. Extending various microphysical EoSs with a maximally stiff EoS, i.e. $v_{\text{sound}} = c$, beyond the central density of a NS with $1.6 M_{\odot}$ determines the highest possible M_{max} for a given $R_{1.6}$ compatible with causality. With Eq. (2) it implies $M_{\text{thres}} \geq 1.22M_{\text{max}}$.

In Fig. 1 the horizontal dark blue band refers to the measured lower limit of M_{thres} given by the total binary mass of GW170817 (Eq. (1)). This GW measurement thus rules out EoSs with very small $R_{1.6}$ because those EoSs would not result in a delayed collapse for the measured binary mass. The allowed range of possible stellar parameters is indicated by the light blue area. The solid blue curve corresponds to the smallest $R_{1.6}$ compatible with Eq. (1). Hence, the radius of a $1.6 M_{\odot}$ NS must be larger than $10.30^{+0.15}_{-0.03}$ km. The error bar corresponds to the radii compatible with the error in M_{tot} . Arguments about the error budget and the robustness are provided in Sect. 3.3.

Figure 1 (right panel) displays $M_{\text{thres}}(M_{\text{max}}; R_{\text{max}})$ for different chosen R_{max} (solid lines). The different sequences for fixed R_{max} are constrained by causality (Koranda et al. 1997; Lattimer & Prakash 2016) requiring

$$M_{\text{max}} \leq \frac{1}{2.82} \frac{c^2 R_{\text{max}}}{G} \quad (5)$$

and with Eq. (3)

$$M_{\text{thres}} \geq 1.23 M_{\text{max}}. \quad (6)$$

The lower bound of M_{thres} given by the measured total mass of GW170817 is shown as dark blue band. The radius R_{max} of the nonrotating maximum-mass NS is thus constrained to be larger than $9.26^{+0.17}_{-0.03}$ km.

Instead of using Eq. (1) it may be more realistic to assume that the remnant was stable for at least 10 milliseconds to yield the observed ejecta properties (high masses, blue component) (Margalit & Metzger 2017; Nicholl et al. 2017; Cowperthwaite et al. 2017). In this case our numerical simulations suggest that $M_{\text{thres}} - M_{\text{tot}} \geq 0.1 M_{\odot}$. This strengthens the radius constraint to $R_{1.6} \geq 10.68^{+0.15}_{-0.04}$ km and $R_{\text{max}} \geq 9.60^{+0.14}_{-0.03}$ km.

Figure 2 shows these radius constraints overlaid on mass-radius relations of different EoSs available in the literature. Our new radius constraints for $R_{1.6}$ and R_{max} derived from GW170817 exclude EoS models describing very soft nuclear matter.

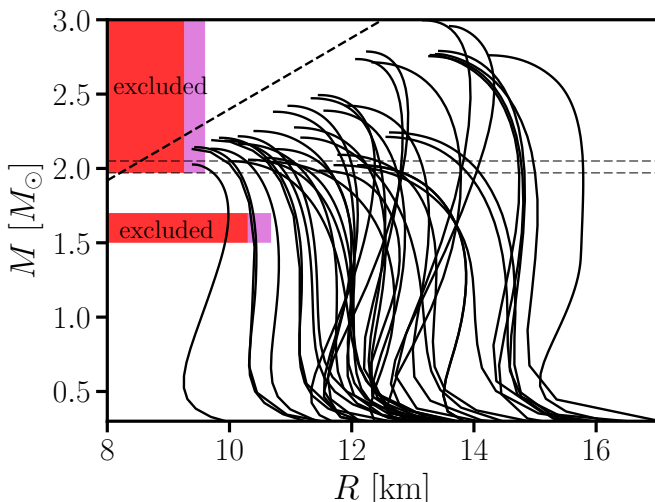


Figure 2. Mass-radius relations of different EoSs with very conservative (red area) and “realistic” (cyan area) constraints of this work for $R_{1.6}$ and R_{max} . Horizontal lines display the lower bound on M_{max} by Antoniadis & et al. (2013). The dashed line shows the causality limit.

3.3. Discussion: robustness and errors

We took an overall conservative approach in this first study. Future refinements may strengthen these constraints. Our way of inferring NS radii is particularly appealing and robust because it only relies on (1) a well measured quantity (total binary mass with reliable error bars), (2) a single verifiable empirical relation (Eqs. (2) or (3)) derived from simulations, and (3) a clearly defined working hypothesis (delayed/no collapse of the merger remnant). All assumptions can be further substantiated and refined by more advanced models and future observations, and error bars can be robustly quantified.

(1) Mass measurement: The total binary mass can be measured with good accuracy and the error bars are given with high confidence. We fully propagate the error through our analysis using the the low-spin prior results of Abbott et al. (2017). If GW170817 was an asymmetric merger as tentatively suggested by the high ejecta mass, the true M_{tot} lies at the upper bound of the error band and our radius constraints become stronger.

(2) Accuracy of empirical relations for M_{thres} : The empirical relations (Eqs. (2) and (3)) are inferred from hydrodynamical simulations (see Bauswein et al. (2013a, 2016); Bauswein & Stergioulas (2017)) and carry a systematic error¹ and an intrinsic scatter (stemming from the sample of candidate EoSs, which do not perfectly fulfill the analytic fit). M_{thres} has been numerically determined with a precision of $\pm 0.05 M_{\odot}$. The deviations between the fits and numerical data are on average less than $0.03 M_{\odot}$ and at most $0.075 M_{\odot}$ ². We do not include this uncertainty in our error analysis because the numerically determined M_{thres} of all tested microphysical candidate EoSs is significantly smaller than the maximum of the $M_{\text{thres}}(M_{\text{max}})$ sequence for the radius given by the respective EoS³. Recall that the maxima of the

¹ The simulations for determining M_{thres} and the corresponding fits employ a conformally flat spatial metric in combination with a GW backreaction scheme (Oechslin et al. 2007; Bauswein et al. 2013a), which results in a slightly decelerated inspiral (compared to fully relativistic calculations) and thus leads to a slight overestimation of M_{thres} by $\sim 0.05 M_{\odot}$. We will quantify this effect in future work and emphasize that a small overestimation implies that our radius constraints are conservative.

² We computed M_{thres} for six additional EoSs not included in Bauswein et al. (2013a) to verify this accuracy in particular for EoS models yielding relatively small NS radii.

³ Within our sample of 17 candidate EoSs the true M_{thres} is on average $0.17 M_{\odot}$ ($0.14 M_{\odot}$ for the R_{max} sequence) below the maximum $M_{\text{thres}}^{\text{up}}$ of the $M_{\text{thres}}(M_{\text{max}}, R)$ relation, which well justifies to neglect the scatter in Eqs. (2) and (3). Three EoSs (eosAU, WFF1, LS375) are relatively close to the maximum ($\sim 0.02 M_{\odot}$ below $M_{\text{thres}}^{\text{up}}$). However, these EoS models become acausal ($v_{\text{sound}} > c$), i.e. unrealistically stiff, at densities of high-

$M_{\text{thres}}(M_{\text{max}})$ sequences are given by maximally (unrealistically) stiff EoSs only constrained by causality. We thus remain conservative by determining minimum NS radii through the maxima of the sequences defined by causality.

We note that evidence for a long-lived merger remnant (e.g. Lippuner et al. 2017; Margalit & Metzger 2017) further strengthens our arguments. The longer the remnant lifetime τ , the larger is the difference $M_{\text{thres}} - M_{\text{tot}} > 0$, which implies stronger radius constraints (see above). These considerations emphasize the importance of a better understanding of the dependence of the remnant life time on the binary mass, which represents a challenge for numerical simulations, but could yield even stronger radius constraints (see Sect. 4). Currently, the life time of presumably more than just a few milliseconds for the remnant in GW170817 implies an additional buffer in our error analysis.

The validity of Eqs. (2) and (3) and their uncertainties should be explored by future simulations employing an even larger set of candidate EoSs and successively improved numerical modeling. It should be checked whether the empirical relations hold for absolutely stable strange quark stars and scenarios involving different families of compact stars.

(3) Distinction of collapse scenarios: The scenario of a delayed/no collapse in GW170817 can be consolidated by more advanced models of the electromagnetic emission involving hydrodynamical merger simulations, nuclear network calculations and radiative transfer calculations. Moreover, we anticipate that as more GW and counterpart observations become available in the future, the comprehension of their emission features will grow and will allow a more robust distinction between prompt and delayed collapse events. The growing understanding can be applied to the interpretation of past events by using additional information about the remnant life time for continuous refinements of the radius constraints. The interpretation of electromagnetic emission resulting from prompt or delayed collapse can be tested in the future also by measuring postmerger GW emission (Clark et al. 2014).

4. FUTURE MEASUREMENTS

Ideas introduced in this paper bear the potential of very strong EoS constraints as they are applied to future GW events with higher binary masses. We point out three future hypothetical scenarios.

mass merger remnants, which artificially increases M_{thres} . For these EoSs we determined M_{thres} with a precision of $\pm 0.025 M_{\odot}$.

(1) If an event with higher chirp mass than in GW170818 is detected and evidence for a delayed/no collapse is found, the lower bound on M_{thres} increases. The dark blue band in Fig. 1 is shifted to higher M_{thres} and NS radii must be larger than implied by GW170817. This is sketched in Fig. 3 for a hypothetical event with $M_{\text{tot}} = (2.9 \pm 0.02) M_{\odot}$.

(2) If an event with a higher chirp mass than in GW170817 and a signature of a prompt collapse is observed, this will establish an upper bound on M_{thres} . Figure 3 shows this case for a hypothetical binary mass of $3.1 M_{\odot}$. This measurement would imply an upper bound on NS radii, here $R_{1.6} \leq 13$ km and $R_{\text{max}} \leq 11.48$ km, and an upper bound on M_{max} ($\sim 2.5 M_{\odot}$ for this hypothetical case). These limits are visualized in Fig. 4. The upper right exclusion region is given by the solution to $M_{\text{tot}} = 3.1 M_{\odot} = (-3.38 \frac{GM_{\text{max}}}{c^2 R_{\text{max}}} + 2.43) M_{\text{max}}$ (Eq. 3). As more detections with different binary masses are made, M_{thres} will be constrained increasingly tighter from above and below. This will limit NS radii, i.e. R_{max} and $R_{1.6}$, and M_{max} to a relatively narrow range. M_{max} will be constrained from above and possibly determined with good accuracy if NS radii can be narrowed down by other even more accurate methods.

(3) Events with an upper bound on the remnant life time establish effectively an upper bound on M_{thres} with similar implications as in the previous scenario. This requires a better understanding of the exact dependence of the life time on binary masses and a reliable way to constrain the life time from observations, both of which can be achieved through improved numerical or analytic models. We sketch a hypothetical case in Fig. 5.

5. CONCLUSIONS

We introduce a new method to constrain NS radii and the maximum mass from GW observations of NS mergers and the observational distinction between a delayed and prompt collapse of the merger remnant. Based on the binary mass measurement of GW170817 and the well justified hypothesis of a delayed/no collapse in this event (e.g. Margalit & Metzger 2017; Metzger 2017; Nicholl et al. 2017), we show that the radius of a $1.6 M_{\odot}$ NS must be larger than $10.68^{+0.15}_{-0.04}$ km and the radius of the maximum-mass configuration, R_{max} , is larger than $9.60^{+0.14}_{-0.03}$ km. We stress the potential of future GW events. In particular, an event associated with a prompt collapse will constrain NS radii from above as well as the maximum mass M_{max} of nonrotating NSs. As the sensitivity of ground-based GW detectors increases, more events with more accurate mass measurements can be expected. Similarly, we anticipate a more robust identification of the collapse behavior as more electromag-

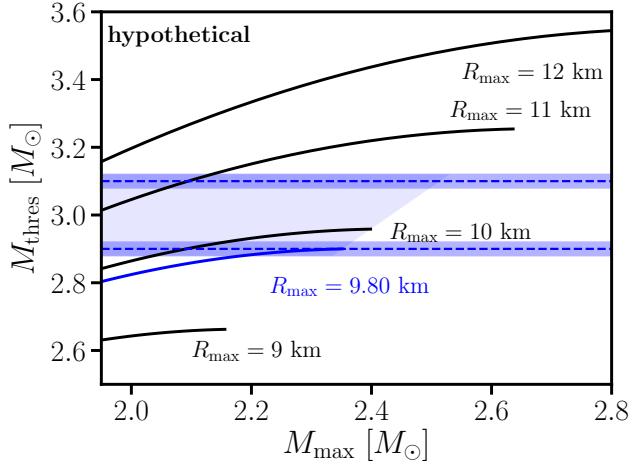


Figure 3. Same as Fig. 1 (right panel). Dark blue bands display binary masses of hypothetical events with $2.9 M_\odot$ resulting in a delayed collapse and $3.1 M_\odot$ resulting in a prompt collapse. Viable NS properties are constrained to the light blue area.

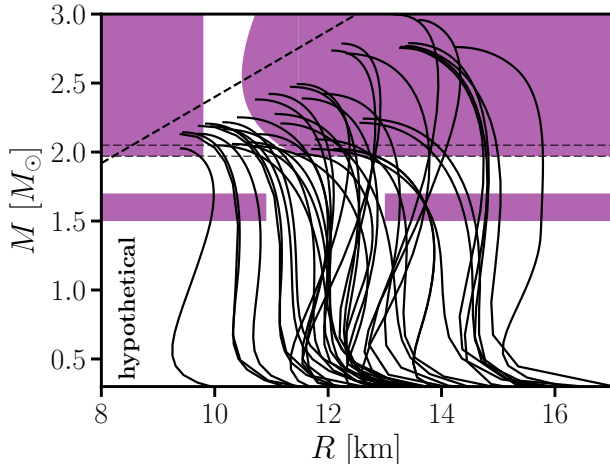


Figure 4. Mass-radius relations of different EoSs with hypothetical exclusion regions (purple areas) from a delayed-collapse event with $M_{\text{tot}} = 2.9 M_\odot$ and a prompt-collapse event with $M_{\text{tot}} = 3.1 M_\odot$ employing the methods of this work (cf. Fig. 3).

netic counterparts are observed and increasingly better understood theoretically.

Our new method is particularly promising because it does not require higher SNRs of future GW events and is thus directly applicable to any new event within the era of current detectors for which the collapse behavior can be classified. It provides a robust, complimentary way of constraining the high-density EoS independent of efforts to measure finite-size effects during the late

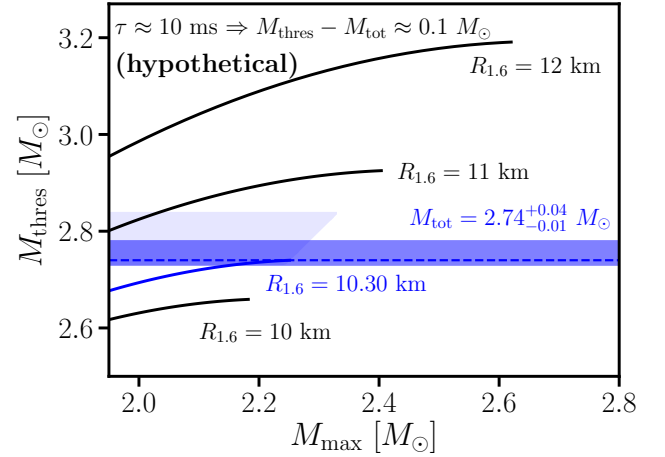


Figure 5. Same as Fig. 1 (left panel) hypothetically assuming evidence for a remnant life time of $\tau \leq 10$ ms in an event like GW170817. NS properties R_{16} and M_{max} would be constrained to the light blue area implying tight bounds on $R_{1.6}$.

inspiral phase (Faber et al. 2002; Flanagan & Hinderer 2008; Read et al. 2013; Del Pozzo et al. 2013; Abbott et al. 2017) or prospects to detect oscillations from the postmerger phase (Bauswein & Janka 2012; Bauswein et al. 2012, 2014; Clark et al. 2014; Chatziioannou et al. 2017).

Apart from the model-dependent interpretation of the electromagnetic emission our method only relies on binary mass measurements and empirical relations describing $M_{\text{thres}}(M_{\text{max}}, R)$. Future calculations can further corroborate these relations for a larger sample of candidate EoSs and with more sophisticated models, although it seems unlikely that for instance a detailed incorporation of neutrinos or magnetic fields can have a significant influence on the relations for the threshold mass. We emphasize the simplicity and robustness of our constraints as a major advantage.

We demonstrated this robustness with the observation of GW170817 and its electromagnetic counterpart making conservative assumptions throughout, for instance by assuming an equal-mass merger. Future work should refine this first study and will yield stronger radius constraints. Specifically we refer to the inclusion of mass-ratio effects and additional information from limits on the remnant life time. As follow-up to this letter we will

update our radius constraints following the methods described here as new measurements become available⁴.

We thank K. Hebeler for EoS tables. A.B. acknowledges support by the Klaus Tschira Foundation. Partial support comes from COST actions GWverse CA16104

and PHAROS CA16214 and from the DAAD Germany-Greece grant ID 57340132. H.-T. J. acknowledges support by the European Research Council through grant ERC AdG 341157-COCO2CASA and by the Deutsche Forschungsgemeinschaft through grants SFB 1258 and EXC 153.

REFERENCES

- Abbott, B. P., Abbott, R., Abbott, T. D., et al. 2017, *Phys. Rev. Lett.*, 119, 161101. <https://link.aps.org/doi/10.1103/PhysRevLett.119.161101>
- Antoniadis, J., & et al. 2013, *Science*, 340, 448
- Baiotti, L., Giacomazzo, B., & Rezzolla, L. 2008, *PhRvD*, 78, 084033
- Bauswein, A., Baumgarte, T. W., & Janka, H.-T. 2013a, *PhRvL*, 111, 131101
- Bauswein, A., Goriely, S., & Janka, H.-T. 2013b, *ApJ*, 773, 78
- Bauswein, A., & Janka, H.-T. 2012, *PhRvL*, 108, 011101
- Bauswein, A., Janka, H.-T., Hebeler, K., & Schwenk, A. 2012, *PhRvD*, 86, 063001
- Bauswein, A., & Stergioulas, N. 2017, *MNRAS*, 471, 4956
- Bauswein, A., Stergioulas, N., & Janka, H.-T. 2014, *PhRvD*, 90, 023002
- . 2016, *European Physical Journal A*, 52, 56
- Chatziioannou, K., Clark, J. A., Bauswein, A. Millhouse, M., Littenberg, T., & Cornish, N. 2017, to be submitted to *PhRvD*
- Chornock, R., Berger, E., Kasen, D., et al. 2017, *ApJL*, 848, L18. <https://arxiv.org/abs/1710.05454>
- Clark, J., Bauswein, A., Cadonati, L., et al. 2014, *PhRvD*, 90, 062004
- Cowperthwaite, P. S., Berger, E., Villar, V. A., et al. 2017, *ApJL*, 848, L17. <https://arxiv.org/abs/1710.05840>
- Del Pozzo, W., Li, T. G. F., Agathos, M., Van Den Broeck, C., & Vitale, S. 2013, *Physical Review Letters*, 111, 071101
- Drout, M. R., Piro, A. L., Shappee, B. J., et al. 2017, *ArXiv e-prints*, arXiv:1710.05443
- Faber, J. A., Grandclément, P., Rasio, F. A., & Taniguchi, K. 2002, *Physical Review Letters*, 89, 231102
- Fernández, R., & Metzger, B. D. 2013, *MNRAS*, 435, 502
- Flanagan, É. É., & Hinderer, T. 2008, *PhRvD*, 77, 021502
- Hotokezaka, K., Kiuchi, K., Kyutoku, K., et al. 2013, *PhRvD*, 87, 024001
- Hotokezaka, K., Kyutoku, K., Okawa, H., Shibata, M., & Kiuchi, K. 2011, *PhRvD*, 83, 124008
- Just, O., Bauswein, A., Pulpillo, R. A., Goriely, S., & Janka, H.-T. 2015, *MNRAS*, 448, 541
- Kasen, D., Metzger, B., Barnes, J., Quataert, E., & Ramirez-Ruiz, E. 2017, *Nature*, 1710.05463. <https://arxiv.org/abs/1710.05463>
- Kasliwal, M. M., Nakar, E., Singer, L. P., et al. 2017, *ArXiv e-prints*, arXiv:1710.05436
- Kilpatrick, C. D., Foley, R. J., Kasen, D., et al. 2017, *ArXiv e-prints*, arXiv:1710.05434
- Koranda, S., Stergioulas, N., & Friedman, J. L. 1997, *ApJ*, 488, 799
- Lattimer, J. M., & Prakash, M. 2016, *PhR*, 621, 127
- LIGO Scientific Collaboration, Virgo Collaboration, & et al. 2017, *ApJL*, 848, L12
- Lippuner, J., Fernández, R., Roberts, L. F., et al. 2017, *MNRAS*, 472, 904
- Margalit, B., & Metzger, B. 2017, *ArXiv e-prints*, 1710.05938v1, arXiv:1710.05938v1
- Metzger, B. D. 2017, *ArXiv e-prints*, 1710.05931v1, arXiv:1710.05931v1
- Metzger, B. D., & Fernández, R. 2014, *MNRAS*, 441, 3444
- Metzger, B. D., Martínez-Pinedo, G., Darbha, S., et al. 2010, *MNRAS*, 406, 2650
- Nicholl, M., Berger, E., Kasen, D., et al. 2017, *ApJL*, 848, L18. <https://arxiv.org/abs/1710.05456>
- Oechslin, R., Janka, H.-T., & Marek, A. 2007, *A&A*, 467, 395
- Oertel, M., Hempel, M., Klähn, T., & Typel, S. 2017, *Reviews of Modern Physics*, 89, 015007
- Özel, F., & Freire, P. 2016, *ARA&A*, 54, 401
- Perego, A., Rosswog, S., Cabezón, R. M., et al. 2014, *MNRAS*, 443, 3134
- Read, J. S., Baiotti, L., Creighton, J. D. E., et al. 2013, *PhRvD*, 88, 044042
- Sekiguchi, Y., Kiuchi, K., Kyutoku, K., Shibata, M., & Taniguchi, K. 2016, *PhRvD*, 93, 124046
- Shibata, M. 2005, *PhRvL*, 94, 201101
- Siegel, D. M., Ciolfi, R., & Rezzolla, L. 2014, *ApJL*, 785, L6

⁴ Updated constraints will be published on <http://wwwmpa.mpa-garching.mpg.de/~bauswein/radiusconstraint/>

Smartt, S. J., Chen, T.-W., Jerkstrand, A., et al. 2017,
ArXiv e-prints, arXiv:1710.05841

Takami, K., Rezzolla, L., & Baiotti, L. 2014, Physical
Review Letters, 113, 091104

Tanaka, M., Utsumi, Y., Mazzali, P. A., et al. 2017,
published in PASJ, 1710.05850.

<https://arxiv.org/abs/1710.05850>

Tanvir, N. R., Levan, A. J., Gonzalez-Fernandez, C., et al.
2017, ArXiv e-prints, 1710.05455, 1710.05455.

<https://arxiv.org/abs/1710.05455>

Wanajo, S., Sekiguchi, Y., Nishimura, N., et al. 2014,
ApJL, 789, L39